GEOCHEMISTRY

Increased fluxes of shelf-derived materials to the central Arctic Ocean

Lauren E. Kipp,[1,2]* Matthew A. Charette,[1] Willard S. Moore,[3] Paul B. Henderson,[1] Ignatius G. Rigor[4]

Rising temperatures in the Arctic Ocean region are responsible for changes such as reduced ice cover, permafrost thawing, and increased river discharge, which, together, alter nutrient and carbon cycles over the vast Arctic continental shelf. We show that the concentration of radium-228, sourced to seawater through sediment-water exchange processes, has increased substantially in surface waters of the central Arctic Ocean over the past decade. A mass balance model for ^{228}Ra suggests that this increase is due to an intensification of shelf-derived material inputs to the central basin, a source that would also carry elevated concentrations of dissolved organic carbon and nutrients. Therefore, we suggest that significant changes in the nutrient, carbon, and trace metal balances of the Arctic Ocean are underway, with the potential to affect biological productivity and species assemblages in Arctic surface waters.

INTRODUCTION

The Arctic Ocean is heavily influenced by margin sources, in part due to the wide continental shelves that make up more than 50% of its area (*1*). Rising temperatures cause shifts in the Arctic system, notably permafrost thawing on land and on continental shelves (*2*), increased river discharge (*3*), and reduced ice cover (*4*); these changes serve to increase the communication between the shelves and the central basin. Permafrost thaw can release solutes from previously frozen mineral soils into groundwater and river waters; evidence of permafrost-derived carbon has recently been observed in river basins of the Eurasian Arctic (*5*). Rivers deliver terrestrial materials including carbon and trace metals to the coastal ocean, some of which are exported to the central Arctic through the Transpolar Drift (TPD) (*6*, *7*). The loss of sea ice will enhance the influence of wind stress on river plumes and coastal waters, which may increase offshore transport (*8*) and lead to upwelling (*9*) and increased turbulence over shelves. Because the transport of shelf-derived nutrients and trace metals to the open ocean is vital in supporting primary productivity, it is important to understand how shelf inputs are changing in response to these drivers.

Radium isotopes are produced through the decay of naturally occurring thorium isotopes in sediments. Unlike thorium, radium is relatively soluble in seawater (*10*); hence, short-lived radium concentrations in ocean surface waters are a first-order indicator of shelf- and margin-derived sediment-water exchange processes. Because thorium isotopes remain largely bound in sediments, ocean margin sediments provide a continuous source of radium, with each radium isotope being regenerated on a time scale determined by its half-life ($T_{1/2}$), such that shorter-lived isotopes are renewed more quickly than longer-lived isotopes. Radium-228 (^{228}Ra; $T_{1/2}$ = 5.75 years) is well suited for monitoring changes in the shelf inputs, because it can integrate over large spatial scales and respond to changes on subdecadal time periods. Hence, this isotope has been applied as a flux gauge for sedimentary trace element inputs (*11*) and used to examine the relative importance of coastal inputs to the Atlantic Ocean, Pacific Ocean, and Indian Ocean basins (*12*). Here, we use ^{228}Ra to show that the flux of materials from shelves to the central Arctic has increased substantially over the past decade, indicating changes in surface water chemistry that could affect primary productivity in this basin.

[1]Department of Marine Chemistry and Geochemistry, Woods Hole Oceanographic Institution, Woods Hole, MA 02543, USA. [2]Massachusetts Institute of Technology–Woods Hole Oceanographic Institution Joint Program in Oceanography/Applied Ocean Science and Engineering, Woods Hole, MA 02543, USA. [3]Department of Earth and Ocean Sciences, University of South Carolina, Columbia, SC 29208, USA. [4]Applied Physics Laboratory and Department of Atmospheric Sciences, University of Washington, Seattle, WA 98105, USA.
*Corresponding author. Email: lkipp17@mit.edu

RESULTS AND DISCUSSION

Radium-228 distribution in surface waters and comparison to historical studies

We measured the distribution of Ra isotopes in the Arctic Ocean from the Chukchi Shelf to the North Pole during the 2015 U.S. GEOTRACES Arctic Transect (GN01). Surface water samples (2 m) were collected at 69 stations (Fig. 1), whereas full water column profiles were obtained from 20 stations (fig. S1). The ^{228}Ra activities measured on the Chukchi

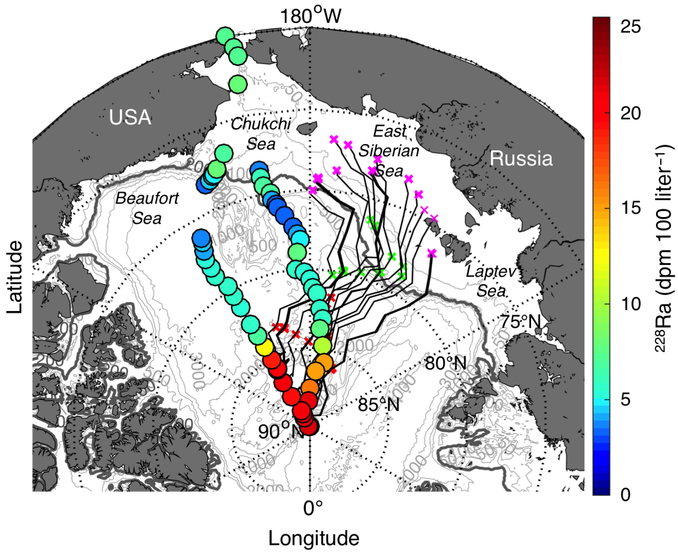

Fig. 1. Radium-228 activities in surface waters (2 m) of the Arctic Ocean. Ice back-trajectories determined for each of the sampling stations are shown in black. The red, green, and magenta symbols indicate the position of the ice 6, 12, and 18 months before each sample was collected, respectively. The 200-m isobath is highlighted in bold.

Shelf were similar to activities measured in 2002 (*13*, *14*); however, in the upper 100 m of the central basin ($n = 30$), ^{228}Ra activities were higher than those observed in 1994 ($n = 7$) (*15*) and 2007 ($n = 11$) (Fig. 2 and figs. S2 and S3) (*16*). A period of abnormally strong and consistent cyclonic circulation conditions preceded sampling in 1994 (*17*), causing the maximum ^{228}Ra activities to be observed farther south (80°N) than in 2007 and 2015 (fig. S4). The 2015 data presented here and the 2007 study completed by Rutgers van der Loeff *et al.* (*16*) are the two most extensive data sets of ^{228}Ra in the central Arctic; thus, we will focus on the comparison between these 2 years.

Ice drift back-trajectories, used here as a proxy for mixed layer water mass transport (*18*), suggest that water above 85°N originated from the East Siberian Arctic Shelf seas (ESAS; Laptev Sea and East Siberian Sea) via the TPD (see Materials and Methods) (Fig. 1 and fig. S5). Radium-228 likely accumulated during the transport of water across the wide and shallow ESAS (*19*, *20*). Ice drift in 2007 followed a similar trajectory (fig. S6); thus, changing source waters cannot explain the difference in activities. In addition, changes due to decay during transit can be ruled out because the transport time from the shelf to the central Arctic was similar in both years: Ice back-trajectories suggest transport times of 4 to 16 months and 8 to 18 months for 2007 and 2015, respectively, and surface water ages based on the ingrowth of thorium-228 (^{228}Th; $T_{1/2}$ = 1.91 years) with ^{228}Ra suggest similar time scales of 6 to 12 months for 2015 and 1 to ≥3 years for 2007 (see Materials and Methods) (fig. S7) (*16*).

A Eurasian shelf source is supported by the relationship of ^{228}Ra with the longer-lived radium-226 (^{226}Ra; $T_{1/2}$ = 1600 years); this shelf endmember has a high ^{228}Ra/^{226}Ra ratio similar to that measured in the TPD (Fig. 3). A strong indication of shelf origin is also evident in the correlation between ^{228}Ra and the meteoric water fraction (Fig. 2). However, this indicator of terrestrial freshwater input was in the same range for 2007 and 2015; thus, increased river discharge cannot fully account for the increase in ^{228}Ra. Therefore, the change must be due to an increase in the input of ^{228}Ra from Arctic shelves.

Sources and sinks of ^{228}Ra in surface waters

Most ^{228}Ra present in the upper 500 m of the ocean is due to shelf inputs (*21*); the 2015 Arctic Ocean ^{228}Ra inventory for this layer is $(6.8 \pm 1.4) \times 10^{23}$ atoms. This inventory was determined by multiplying the average of the individual station inventories [$(7.1 \pm 1.4) \times 10^{10}$ atoms m^{-2}; fig. S8] by the area of the Arctic as defined by Jakobsson (*1*) (9.54×10^{12} m^2) (fig. S8) (see Materials and Methods). Because this study provides an extensive data set of ^{228}Ra in the upper water column, this inventory estimate is fairly robust. However, it is biased toward Western Arctic activities and could be improved with inventory measurements in the Eastern Arctic.

Arctic Ocean removal processes (sinks) for ^{228}Ra include loss via radioactive decay and transport from the Arctic basin. Applying the decay rate (0.12 year^{-1}) to the ^{228}Ra inventory yields a loss of 8.2×10^{22} atoms year^{-1} [estimated range of 6.6×10^{22} to 9.9×10^{22} atoms year^{-1} (see Materials and Methods)]. The transport loss of ^{228}Ra is estimated by dividing the inventory of ^{228}Ra by the residence time of surface water, approximately 3 to 10 years (*22*). For a conservative estimate, we use 10 years, resulting in a sink of 6.8×10^{22} atoms year^{-1} (5.4×10^{22} to 1.6×10^{23} atoms year^{-1}). Thus, the total loss of ^{228}Ra from the surface ocean is 1.5×10^{23} atoms year^{-1} (1.2×10^{23} to 2.6×10^{23} atoms year^{-1}).

At steady state, the ^{228}Ra sinks are balanced by upper ocean sources. Sediments transported by ice to the central Arctic basin are a potential source of ^{228}Ra to the surface layer. Samples of ice containing visible sediment were collected on the GN01 transect, and ^{228}Ra activities were measured in the melted ice and sediment fractions (see Materials and Methods). The highest sediment activity measured was 3.1 ± 0.3 dpm g^{-1} [$(1.3 \pm 0.1) \times 10^7$ atoms g^{-1}] (table S2), and 21% of the ^{228}Ra desorbed upon ice melting, although this percentage could vary depending on salinity and sediment properties. This sediment activity is similar to that measured on suspended and bottom sediments of the Amazon River [2 to 3 dpm g^{-1} (*23*)] and suspended sediments collected from the Mackenzie River [2.9 dpm g^{-1} (see Materials and Methods)]. The concentration of ice-rafted debris in the central Arctic is thought to vary between 8 and 84 metric tons km^{-2} (*24*), and seasonal ice melt equals $\sim 1.0 \times 10^7$ km^2 (the average difference in September-March ice extent for 2010–2015; NOAA Sea Ice Index, Version 2). Using an average ice sediment concentration of 32 metric tons km^{-2} and assuming 21% of the ^{228}Ra desorbed from the sediments upon melting, we estimate the flux of ^{228}Ra

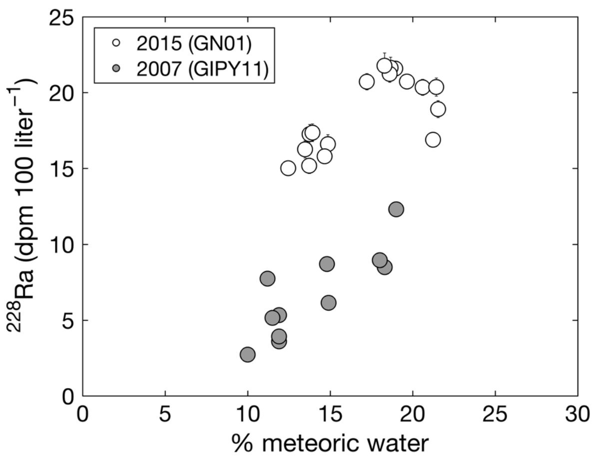

Fig. 2. Radium-228 activities in surface waters (<50 m) above 85°N as a function of percent meteoric water. Open symbols represent samples collected in 2015 on the GN01 transect, and closed symbols represent samples collected in 2007 on the GIPY11 transect (*16*). Error bars for the data collected in 2007 are smaller than the symbols.

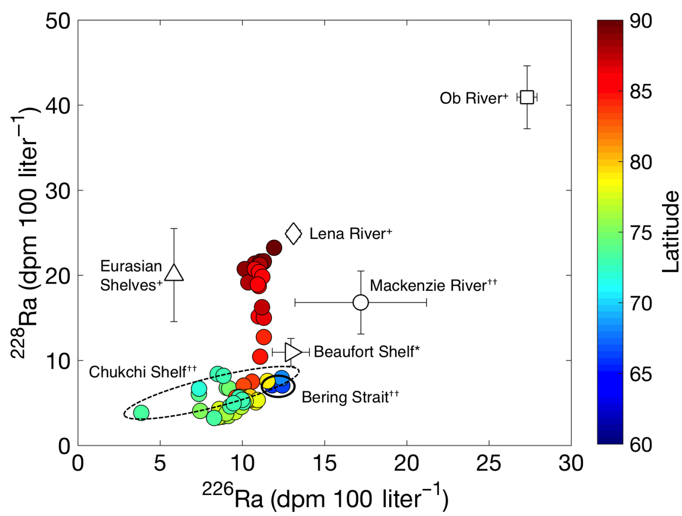

Fig. 3. Activities of ^{228}Ra and ^{226}Ra measured in surface waters in 2015 (circles), shown with historical measurements of shelf and river endmembers. Error bars for the 2015 data are smaller than the symbols. ⁺⁺This study; ⁺Rutgers van der Loeff *et al.* (*19*); *Smith *et al.* (*15*).

from ice-rafted sediments to be 8.9 × 10^{20} atoms year^{-1} (1.2 × 10^{20} to 4.0 × 10^{21} atoms year^{-1}). Although there is significant spatial and temporal variability associated with this source, this input is <1% of the flux of ^{228}Ra to the surface layer.

Rivers supply ^{228}Ra to the ocean through the fresh water dissolved load and desorption of ^{228}Ra from suspended particles in the river estuaries (*23*). To investigate the dissolved river flux of ^{228}Ra to the Arctic, we collected bimonthly water samples from the Mackenzie River in Tsiigehtchic, Northwest Territories, Canada, from April 2015 to June 2016 (fig. S9). The average measured ^{228}Ra activity, 16.8 ± 3.7 dpm 100 liter^{-1}, is similar to activities measured in the Lena River in September 1999 (11.1 to 24.9 dpm 100 liter^{-1}) but significantly lower than the activity measured in the Ob River in September 1999 (40.9 ± 3.7 dpm 100 liter^{-1}) (*19*). The weighted average dissolved ^{228}Ra in major Arctic rivers was determined to be 24 ± 13 dpm 100 liter^{-1} based on the activities and discharge of these three rivers (see Materials and Methods). Scaling this activity by total Arctic river runoff [(4.2 ± 0.42) × 10^{12} m^3 year^{-1} (*25*)] yields a dissolved ^{228}Ra flux of 4.4 × 10^{21} atoms year^{-1} (1.8 × 10^{21} to 7.4 × 10^{21} atoms year^{-1}). However, this may be an overestimate because Ra removal through flocculation during estuarine mixing has been observed in the Lena River and Ob River (*19*), in contrast to the excess ^{228}Ra observed in the Mackenzie River estuary (fig. S10).

The flux of ^{228}Ra due to desorption from riverine particles was examined through sampling across the salinity gradient of the Mackenzie River estuary in June 2016. The activity of ^{228}Ra measured in suspended riverine particles in the Mackenzie River was 2.9 ± 0.3 dpm g^{-1}, and approximately 32% desorbed during estuarine mixing (fig. S10) (see Materials and Methods). Scaling these values by the total sediment delivery from 13 of the largest Arctic rivers [2.8 × 10^{14} g year^{-1} (*26*)] yields a river particle desorption flux of 1.1 × 10^{21} atoms year^{-1} (2.5 × 10^{20} to 2.5 × 10^{21} atoms year^{-1}). Thus, the total riverine source is 5.5 × 10^{21} atoms year^{-1} (2.0 × 10^{21} to 9.9 × 10^{21} atoms year^{-1}) or about 4% of the total surface loss terms. There are significant seasonal variations in ^{228}Ra (fig. S9), as well as river sediment and water discharge (*26*), although they are unlikely to make Arctic rivers a major contributor to the surface ^{228}Ra inventory.

Inflowing Pacific Ocean and Atlantic Ocean waters supply ^{228}Ra to the surface Arctic Ocean. The Pacific inflow was estimated by multiplying the ^{228}Ra activity measured in the Bering Strait on the GN01 transect (7.05 ± 0.02 dpm 100 liter^{-1}; 1σ, n = 2) by the volume transport, (3.5 ± 0.3) × 10^{13} m^3 year^{-1} (*27*). Whereas the Bering Strait inflow is well constrained, ^{228}Ra activities in the Bering Sea may vary seasonally as a result of physical processes over the shelf such as deep winter mixing. The Atlantic inflow is more difficult to constrain, but because the ^{228}Ra activities are relatively low, variations in this source will not significantly change its contribution to the surface ^{228}Ra inventory. The addition of ^{228}Ra from Atlantic inflow was determined using historical ^{228}Ra measurements in the Greenland Sea and Norwegian Sea (*28*) (1.35 ± 0.72 dpm 100 liter^{-1}; 1σ, n = 14) and a transport rate of 2.0 × 10^{14} m^3 year^{-1} (estimated range of 1.4 × 10^{14} to 2.1 × 10^{14} m^3 year^{-1}) through the Fram Strait and Barents Sea (*29*). Thus, the total input of ^{228}Ra through advection is 2.2 × 10^{22} atoms year^{-1} (1.4 × 10^{22} to 3.1 × 10^{22} atoms year^{-1}), accounting for 15% of the total ^{228}Ra input to the surface layer.

The combination of sources above leaves approximately 80% of the total ^{228}Ra input unaccounted for (1.2 × 10^{23} atoms year^{-1}, estimated range of 7.5 × 10^{22} to 2.5 × 10^{23} atoms year^{-1}; Table 1). The only other source with a ^{228}Ra inventory large enough to close the ^{228}Ra budget is continental margin sediments. The sharp increase in ^{228}Ra activities observed between 2007 and 2015 indicates that the inputs of ^{228}Ra to Arctic surface waters are not currently in steady state; if shelf sediments are the major source of ^{228}Ra to surface waters, then this implies radical changes in near-shore sediment-water exchange processes.

Changing shelf inputs

Shelf processes that could supply significant amounts of ^{228}Ra to the water column include coastal erosion, permafrost thaw, and increased exchange between shelf sediments and overlying waters. Coastline erosion rates on the ESAS are some of the highest in the Arctic (*30*) and are rising due to increased storm frequency and higher air and sea temperatures (*31*). The amount of sediment added to the Arctic Ocean due to erosion is estimated to be 4.3 × 10^8 metric tons year^{-1} (*32*). Assuming that the ^{228}Ra activity of coastal sediments is the same as that of the suspended sediments measured in the Mackenzie River (2.9 ± 0.3 dpm g^{-1}) and that the same percentage desorbs when sediments are added to the ocean (32%), the amount of ^{228}Ra added to the coastal ocean via erosion is on the order of 1.7 × 10^{21} atoms year^{-1}. The addition of ^{228}Ra from this process alone appears to be too small to close the ^{228}Ra budget.

Permafrost contains a reservoir of Ra that may be liberated as a consequence of deepening active layers (*2*) and a higher frequency and

Table 1. Radium-228 sources and sinks (all in 10^{22} atoms year^{-1}) in the Arctic surface ocean. The shelf flux was determined by difference, assuming that, at steady state, the sources of ^{228}Ra to the surface layer must be balanced by sinks. The best estimate for each term was used in the mass balance calculation; see Materials and Methods for details on how the minimum and maximum flux estimates were determined.

Sinks	Best-estimate flux (10^{22} atoms year^{-1})	Minimum flux (10^{22} atoms year^{-1})	Maximum flux (10^{22} atoms year^{-1})	% of total sinks
Decay	8.2	6.6	9.9	55
Advection	6.8	5.4	16	45
Sources	**Best-estimate flux (10^{22} atoms year^{-1})**	**Minimum flux (10^{22} atoms year^{-1})**	**Maximum flux (10^{22} atoms year^{-1})**	**% of total sources**
Ice-rafted sediment	0.089	0.012	0.40	<1
Advection	2.2	1.4	3.1	15
Rivers	0.55	0.20	0.99	4
Shelf	12	7.5	25	81

magnitude of coastal and inland thermokarst processes (*33*, *34*). The transport of solutes liberated through permafrost thaw has been observed on catchment-wide scales (*35*) and could result in an increase in solute fluxes, including ^{228}Ra, to Arctic shelf seas (*5*). Measurements of ^{228}Ra in permafrost collected from Inuvik and Tuktoyaktuk, Northwest Territories, Canada, show that ^{228}Ra activities in permafrost sediments (2.5 ± 0.4 dpm g^{-1}; 1σ, $n = 4$) are higher than those in the active (seasonally thawed) layer (1.5 ± 0.5 dpm g^{-1}; 1σ, $n = 6$) (see Materials and Methods). To our knowledge, these are the first Ra measurements in permafrost. Further studies on the spatial variability and desorption of radium isotopes from permafrost sediments are needed to estimate the magnitude of this source in the Arctic Ocean Ra budget under changing climate conditions. In addition to mobilization in runoff and river discharge, solutes can be transported to the coast through submarine groundwater discharge, which has been observed on the Laptev Shelf (*36*) and may increase in the future as permafrost coverage is reduced (*37*), though the spatial variability of this source is poorly constrained.

Because of the large reservoir of Ra in shelf sediments, enhanced wind-driven vertical mixing over the shelves, a result of sea ice loss and a longer open-water season (*38*), has perhaps the greatest potential to affect the ^{228}Ra budget. Over the inner ESAS, this process has the potential to increase sediment-water exchange over an extensive area. During the 5-year period preceding the 2015 survey, parts of the Laptev Sea experienced twice as many ice-free days as the 5-year period preceding the 2007 study (fig. S11), supporting the possibility for increased vertical mixing over the shelf between 2011 and 2015. The loss of ice cover and the presence of more mobile ice cause more surface stress, leading to increased vertical mixing, as well as upwelling and/or downwelling over the shelf (*8*); these vertical exchange processes bring ^{228}Ra sourced from shelf sediments to surface waters. In addition, the retreat of the ice edge beyond the shelf break allows for wind-driven upwelling of deeper slope waters onto the shelf (*9*), which could transport additional ^{228}Ra released from slope sediments (such as the ^{228}Ra plumes observed off the Chukchi Slope; fig. S1) to the surface. This mechanism of enrichment may also explain why activities over the Chukchi Shelf have not increased between 2002 (*13*) and 2015, because there has not been a significant change in the number of ice-free days over this shelf in the past decade (fig. S11).

Shelf inputs are also supported by the ^{226}Ra activities measured in 2007 and 2015 (figs. S12 and S13). Because of the longer half-life of ^{226}Ra, this isotope has a larger inventory in surface waters, and a substantial change in inputs is required to shift the observed activities. ^{226}Ra is also regenerated more slowly in shelf sediments such that a ^{228}Ra/^{226}Ra flux ratio greater than 1 is typical of a shelf sediment pore water source; ratios as high as 3.9 have been observed over the Laptev Shelf (*19*). Ratios between 0.9 and 2.1 were observed in the TPD in 2015 (Fig. 3), whereas the maximum ratio recorded in 2007 was 1.3 (*16*). The smaller increase in ^{226}Ra over this time period compared to ^{228}Ra is consistent with shelves being a relatively larger source of ^{228}Ra; thus, the major change in ^{228}Ra cannot be fully explained by a process that would affect both Ra isotopes in the same way (such as changes in biological uptake, remineralization, or coastal erosion). A longer residence time over the shelf could also increase the activities of both Ra isotopes in surface waters, but a doubling of the ^{228}Ra inventory over the shelf would require a similar increase in the shelf water residence time. This is unlikely given the rising freshwater fluxes to the shelves (*3*) and increasing wind stress resulting from longer open-water seasons (*8*).

On the basis of these two data sets alone, we cannot conclusively determine the mechanism driving increased shelf inputs. Measurements of ^{228}Ra over the shelves and in the central Arctic must be collected over multiple years and seasons to elucidate the temporal variability of this tracer, and more data from the endmember shelf seas are needed to constrain the spatial variability of the shelf source.

This study provides the first direct estimate of the Arctic shelf flux of ^{228}Ra, which will act as an important baseline with which future changes in Arctic shelf-basin exchange can be monitored. Although the current flux is similar to that in other ocean basins (Fig. 4A) (*12*), it is apparent that shelf inputs have a disproportionately large impact in the Arctic when normalized to basin area (Fig. 4B). The increase in the supply of ^{228}Ra to the central Arctic implies that the fluxes of other shelf-derived species, including carbon, nutrients, and trace metals, must also be rising, with the potential for significant changes to the biogeochemistry of the central basin, as shelf waters are eventually transported to the central Arctic via the TPD. Historical observations of dissolved organic carbon and dissolved iron concentrations in the central Arctic show that these species are elevated in the TPD (*6*, *7*). Varying nutrient and trace metal concentrations in the TPD will have a direct impact on primary productivity because this pathway delivers nutrients directly to the surface layer; if concentrations increase significantly, then this intensified source may minimize the importance of the vertical mixing supply of nutrients from deep water. At present, productivity is low in the central Arctic due to both light and nutrient limitations (*39*). However, decreasing sea ice coverage will increase primary productivity and

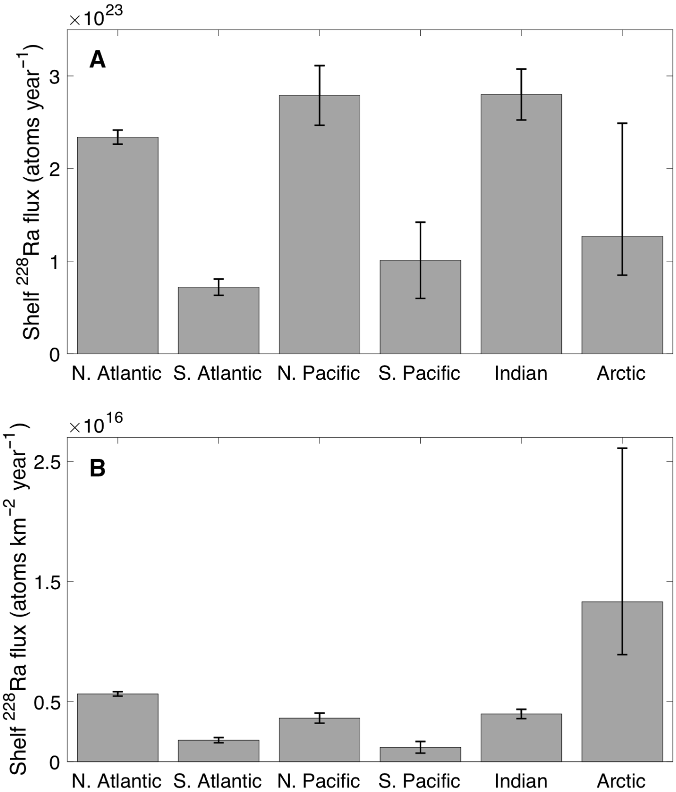

Fig. 4. The coastal flux of ^{228}Ra to each ocean basin. The flux is shown (**A**) in atoms year^{-1} and (**B**) normalized to the area of each basin in atoms km^{-2} year^{-1}. The fluxes from basins other than the Arctic are from Kwon *et al.* (*12*), and areas are from the ETOPO1 surface relief model (*56*). The area of the Arctic basin is from Jakobsson (*1*).

allow for a longer growing season (*40*); growth will also be supported by rising nutrient fluxes. Changing light and nutrient conditions may cause shifts in the dominant plankton species in surface waters, which in turn could affect higher trophic levels including fish species and marine mammals (*41*, *42*). Continued monitoring of shelf inputs to Arctic surface waters is therefore vital to understanding how the changing climate will affect the chemistry, biology, and economic resources of the Arctic Ocean.

MATERIALS AND METHODS

Surface sample collection and processing

Surface water Ra samples (280 liters) were collected from ~2 m using a submersible surface pump and filtered through a MnO_2-coated acrylic fiber, which quantitatively scavenges Ra from the seawater. Fiber samples were then ashed in a muffle furnace at 820°C for 24 hours and the fiber ash was transferred to polystyrene vials, sealed with epoxy (to prevent ^{222}Rn loss), aged for at least 3 weeks, and counted on a high-purity, well-type germanium detector to measure ^{228}Ra, using the lines for ^{228}Ac (338 and 911 keV), and ^{226}Ra, using the line for ^{214}Pb (352 keV). Detector efficiency was determined by measuring ashed fiber standards prepared with a standard solution containing ^{226}Ra and ^{232}Th with daughters in equilibrium. Analytical uncertainties are reported as 1σ.

Water column sample collection and processing

Water column Ra samples were collected using McLane in situ pumps (McLane WTS-LV) deployed on a 9.5 mm plastic-coated Vectran line. Seawater was filtered through 1-μm filters to remove particles and then pumped through a MnO_2-coated cellulose cartridge to collect dissolved Ra, Th, and Ac isotopes [see Henderson *et al.* (*43*) for details of cartridge preparation]. Pumps were programmed to run for 4 hours, typically filtering 1200 to 1600 liters of seawater at an average flow rate of 5.6 liters min^{-1}. After collection, cartridges were rinsed with Ra-free fresh water and dried with filtered compressed air to remove excess moisture. To determine the cartridge scavenging efficiencies, we collected small-volume samples of ^{226}Ra (15 to 25 liters) using a Niskin bottle mounted either on the CTD (conductivity, temperature, and depth) rosette (shallow casts) or above the pumps (deep casts), and the activities of Ra measured on these samples were compared to those determined on the cartridges.

Cartridges were ashed and analyzed by γ spectrometry using the same method as the surface samples. Detector efficiencies were determined using ashed cartridge standards, and analytical uncertainties are reported as 1σ.

The small-volume ^{226}Ra samples were filtered through MnO_2-coated acrylic fibers. Fibers were then rinsed with Ra-free fresh water, partially dried, and sealed in a fiber housing for at least 2 weeks to allow for ^{222}Rn ingrowth. Samples were analyzed for ^{226}Ra via ^{222}Ra emanation and scintillation counting (*44*). On average, samples were counted for approximately 230 min, resulting in an analytical error of less than 5%. Fiber standards containing 20 dpm ^{226}Ra (National Institute of Standards and Technology–certified) were analyzed in the same way as the samples at least once every 2 weeks; standard reproducibility was ~3%.

Comparisons between the unfiltered surface samples and the filtered near-surface samples revealed no consistent differences between filtered and unfiltered samples. The Charette and Moore (GN01) and Rutgers van der Loeff (GIPY11) laboratories participated in the 2008 GEOTRACES intercalibration exercise and good agreement was found among the ^{228}Ra activities measured by all three laboratories (*45*).

Ice back-trajectories

The origin of the ice at each of the stations in the central Arctic was determined using back-trajectories of buoys deployed on sea ice and the open ocean as part of the International Arctic Buoy Program (http://iabp.apl.washington.edu/). The average lifetime of a buoy is ~2 years, and there are typically 20 to 30 buoys drifting on pack ice at any given time. The location of each buoy is transmitted to the Argos or Iridium satellite system, which can determine the geographic position of the buoy with an accuracy of ≤300 m (*46*). Sea ice motion was determined using monthly displacements as described in Rigor *et al.* (*46*) and was projected back in time 36 months or until the buoy reached the coast. The estimated error on the back-trajectories is ~100 km year^{-1} (*47*).

We assume that the trajectories of ice drift are representative of large-scale circulation features of surface waters, such as the TPD and Beaufort Gyre (*18*). Ekman transport may also affect the movement of surface waters; at 7 m (the depth of sample collection in 2007), this may cause a ~35° offset between the ice and water movement (*48*).

Surface water age

Surface water transport times from the shelf to the location of sampling were estimated using ice back-trajectories by determining the number of months elapsed since the ice was over the shelf (<200 m). For the 2007 data, this yielded a transport time of 4 to 16 months; the estimated transport time in 2015 was 8 to 18 months.

Surface water ages were also determined through the ingrowth of ^{228}Th, using the model derived by Rutgers van der Loeff *et al.* (*16*) and briefly described here. Radium-228 decays to ^{228}Th, which is particle-reactive and efficiently scavenged in coastal waters; this results in low ^{228}Th/^{228}Ra activity ratios over continental shelves. Once water is advected off the shelf, decreased scavenging rates allow ^{228}Th to grow toward equilibrium with its parent, ^{228}Ra. Thus, the ^{228}Th activity away from the shelf (^{228}Th$_t$) can be determined using Eq. 1

$$({}^{228}\mathrm{Th_t}) = ({}^{228}\mathrm{Th_0})\mathrm{e}^{-(\lambda_{\mathrm{Th}}+\lambda_{\mathrm{s}})t} + \frac{\lambda_{\mathrm{Th}}}{\lambda_{\mathrm{Th}}+\lambda_{\mathrm{s}}-\lambda_{\mathrm{Ra}}}({}^{228}\mathrm{Ra_0})(\mathrm{e}^{-\lambda_{\mathrm{Ra}}t} - \mathrm{e}^{-(\lambda_{\mathrm{Th}}+\lambda_{\mathrm{s}})t}) \tag{1}$$

where λ_s is the scavenging rate constant once the water parcel leaves the shelf, ^{228}Th$_0$ and ^{228}Ra$_0$ are the initial ^{228}Th and ^{228}Ra activities over the shelf, λ_{Th} and λ_{Ra} are the ^{228}Th and ^{228}Ra decay constants, and t is the time since the water parcel has left the shelf.

The activities of ^{228}Ra and ^{228}Th over the shelf were determined by finding the average activity of the surface samples collected at stations over the Chukchi Sea shelf (bottom depth <50 m; n = 4). The average ^{228}Ra activity was 7.17 ± 0.52 dpm 100 liter^{-1}, and the average ^{228}Th activity was 0.26 ± 0.28 dpm 100 liter^{-1}, corresponding to a ^{228}Th/^{228}Ra activity ratio of 0.04 ± 0.04 (1σ). This value is in agreement with previous studies: Kaufman *et al.* (*49*) noted that the ratio is typically <0.05 in coastal waters, Kadko and Muench (*13*) observed a ratio of <0.06 in Bering Strait inflow, and Lepore and Moran (*50*) observed ratios of 0.2 ± 0.2 and 0.1 ± 0.1 over the Chukchi shelf break in the summers of 2002 and 2004, respectively. Rutgers van der Loeff *et al.* (*16*) used a slightly higher shelf ratio of 0.15 ± 0.05 to calculate the age of waters originating over the Eastern Arctic shelves and noted that the model is not very sensitive to the initial ratio. A higher initial ratio would result in shorter transport times.

The scavenging rate constant is estimated using the ^{234}Th-^{238}U parent-daughter pair, with the assumption that the scavenging rate is the same for both Th isotopes. Equation 2 was used to determine the scavenging rate based on the ^{234}Th/^{238}U ratio observed in the shallowest samples from each station (5 m depth)

$$\lambda_s = \frac{\lambda_{234\mathrm{Th}}(1 - {}^{234}\mathrm{Th}/{}^{238}\mathrm{U})}{{}^{234}\mathrm{Th}/{}^{238}\mathrm{U}} \tag{2}$$

where λ_s is the scavenging rate constant, $\lambda_{234\mathrm{Th}}$ is the ^{234}Th decay constant, and ^{234}Th and ^{238}U are the activities of total ^{234}Th and dissolved ^{238}U, respectively.

Because the ^{234}Th/^{238}U ratio varied along the GN01 transect, we used the range in the observed ratios to determine the range of possible scavenging rates. Above 85°N, the average scavenging rate was 0.43 ± 0.46 year^{-1} (1σ); for the rest of the stations north of the shelf (stations 14 to 57), the minimum scavenging rate was 0 year^{-1}, and the maximum rate was 1.07 year^{-1}. Using these rates, the age of the water above 85°N was determined to be in the range of 0.52 to 0.95 years (6 to 12 months) (fig. S7). The ages derived from the ^{228}Th/^{228}Ra model are in agreement with those determined from the ice back-trajectories (8 to 18 months).

Using the ^{228}Th/^{228}Ra ingrowth model, Rutgers van der Loeff *et al.* (*16*) estimated the age of the surface waters in the TPD in 2007 to be 1 to ≥3 years. This is slightly longer than the transport time based on ice drift. Both the ice back-trajectories and ^{228}Th/^{228}Ra ingrowth model require assumptions, but the generally good agreement between both methods and both years suggests that the surface water transport times in 2007 and 2015 were not drastically different. Because the difference in ^{228}Ra activities measured in these 2 years is about a factor of 2, it would require a difference in transport time equal to one half-life, or 5.75 years, to explain the offset; on the basis of the transport times derived here, we do not think this is likely.

Meteoric water fraction

Assuming that the four main water masses present in the Arctic (Pacific, Atlantic, meteoric, and sea ice melt waters) have consistent and distinct properties, the contribution of each to the water sampled on the GN01 transect was determined using a system of linear equations. The properties of salinity, δ^{18}O, and nutrient concentrations were used to differentiate the contributions using the endmember compositions and "Arctic N-P" tracer method of Newton *et al.* (*51*). The meteoric water fractions for the GIPY11 cruise in 2007 were determined by Bauch *et al.* (*52*) using the same approach but slightly different endmember nutrient concentrations. Using the GN01 endmembers for the GIPY11 data set would result in a difference of <1.2% in the calculated meteoric water fraction.

Surface water inventory of ^{228}Ra

The ^{228}Ra inventory in surface waters was calculated using 10 stations in the central basin (bottom depth >1000 m) where water column data for the upper 500 m were available (table S1). Two stations with bottom depths of >1000 m were excluded from the inventory calculation due to poor sampling resolution. A depth threshold of 500 m was chosen because ^{228}Ra released from deep sea sediments is unlikely to reach the top 500 m (*21*); thus, any ^{228}Ra present in this layer must be from one of the margin sources included in the mass balance (rivers, ice-rafted sediments, advection, and continental shelves). Depth-integrated inventories were calculated for each station by summing the products of the average activity of two consecutive samples and the depth interval between those samples.

Mass balance model: Sinks

Decay

The decay rate of ^{228}Ra is 0.12 year^{-1}; multiplying this rate by the surface inventory of ^{228}Ra, $(6.8 \pm 1.4) \times 10^{23}$ atoms, results in a loss of 8.2×10^{22} atoms year^{-1}. As the decay rate of this isotope is well characterized, the uncertainty in this sink is a function of the error in the inventory estimate alone. The variability in the decay estimate was assessed using the SD in the ^{228}Ra inventory, resulting in a range of 6.6×10^{22} to 9.9×10^{22} atoms year^{-1}.

Transport

The range in the ^{228}Ra transport sink (5.4×10^{22} to 1.6×10^{23} atoms year^{-1}) was determined by subtracting the SD from the inventory and using a residence time of 10 years to find the minimum loss, and adding the SD to the inventory and using a residence time of 5 years to find the maximum loss. We used a lower limit of 5 years for the residence time because the ^{228}Ra inventory was determined for the upper 500 m of the water column, which includes both the surface mixed layer (residence time of 3 to 5 years) and part of the halocline (residence time of ~10 years) (*22*). In addition, the tritium-helium age method used to determine the residence time likely underestimates the age of the surface layer, where some gaseous ^{3}He may have escaped to the atmosphere. Because of the range in possible residence times, the transport sink estimate is less robust than the decay term. For a conservative shelf flux estimate, we used a residence time of 10 years in the model; using a shorter residence time would result in a larger sink and require a greater flux of ^{228}Ra from the shelves to close the mass balance.

Mass balance model: Sources

Ice-rafted sediment

Two samples of ice containing visible sediment were collected near 88°N during the GN01 transect. Ice was allowed to melt, and samples were stored for approximately 1 year to allow for ^{228}Ra equilibration between the sediment and water phases. The melted ice and sediment fractions were separated by decanting the water and drying the sediments. The water was filtered through a small amount of MnO_2-coated fiber, and the fiber was packed and epoxied in a small vial for direct measurement on a γ detector. The activities of ^{228}Ra and ^{226}Ra were measured in both the melted ice and sediment fractions, using the lines for ^{228}Ac (911 keV) and ^{214}Pb (352 keV) for ^{228}Ra and ^{226}Ra, respectively. Detector efficiencies were determined with a fiber standard spiked with a solution of known ^{228}Ra and ^{226}Ra and prepared in the same geometry as the sample. The activity of ^{228}Ra in the sediments was determined to be 3.1 ± 0.3 dpm g^{-1} and 2.0 ± 0.1 dpm g^{-1}, and the activities in the corresponding melted ice samples were 0.55 ± 0.17 dpm liter^{-1} and below our detection limits, respectively (table S2). To determine the amount of ^{228}Ra that desorbed from ice-rafted sediments, the melted ice activity was converted to units of disintegrations per minute per gram by dividing the activity by the volume of water filtered and multiplying the quotient by the amount of sediment present, and then, this activity was divided by the activity measured in the sediments. The ^{226}Ra activities of the sediments were 1.4 ± 0.1 dpm g^{-1} and 2.3 ± 0.1 dpm g^{-1}, and the respective melted ice activities were 0.38 ± 0.15 dpm liter^{-1} and 0.41 ± 0.09 dpm liter^{-1} (table S2). Baskaran (*53*) observed similar ^{226}Ra activities in ice-rafted sediments collected in the Canada Basin in 2000 (1.76 to 2.17 dpm g^{-1}).

A sample of surface sediments was also collected from the Chukchi Shelf on the GN01 transect (68.0900°N, −168.1055°E) using a multicorer device, and ^{228}Ra and ^{226}Ra activities were measured on the dried sediments. Six aliquots of sediment (~5 g each) were analyzed using high-purity, well-type germanium γ detectors, and the average activity of the six samples was 1.1 ± 0.2 dpm ^{228}Ra g^{-1} and 1.2 ± 0.1 dpm ^{226}Ra g^{-1}. The suspended sediments collected in the Mackenzie River in 2016 had ^{228}Ra and ^{226}Ra activities of 2.9 ± 0.3 dpm g^{-1} and 3.2 ± 0.1 dpm g^{-1}, respectively. On the basis of these other measurements of ^{228}Ra and ^{226}Ra in Arctic sediments, we conclude that the ^{228}Ra activities measured in the ice-rafted sediment samples are reasonable and possibly even on the upper limit of what we would expect for Arctic sediments.

For the mass balance calculation, we used the higher activity (3.1 ± 0.3 dpm ^{228}Ra g^{-1}) and propagated the errors on the melted ice and sediment fractions with the SD in the amount of ice melt [(1.02 ± 0.08) × 10^{7} km^{2} year^{-1}; NOAA Sea Ice Index, Version 2] and the range in possible ice-rafted sediment concentrations [8 to 71 metric tons km^{-2} (*24*)] to determine a final range of 1.2 × 10^{20} to 4.0 × 10^{21} atoms year^{-1}. This range of ice-rafted sediment concentration was determined from samples collected during a transect from the Chukchi Sea to the central Arctic (similar to the path of the GN01 expedition). On the basis of the patterns of ice drift in 2015 (Fig. 1), it is possible that the ice sampled on the GN01 transect may have formed in the Laptev Sea or East Siberian Sea; ice-rafted sediment concentrations in the Laptev Sea have been found to vary between 9 and 45 metric tons km^{-2} (average of 16 metric tons km^{-2}) (*54*), which is within the range used here.

Rivers

Bimonthly river water samples were collected from the Mackenzie River in Tsiigehtchic, Northwest Territories, Canada, between April 2015 and June 2016. A 20-liter sample of surface water was collected, and suspended sediments were allowed to settle overnight. Approximately 1 liter of water was drained to remove most of the suspended sediments, and then, the remaining water was filtered through a raw acrylic fiber to remove most remaining sediment and through a MnO_2-coated acrylic fiber to collect Ra. Fiber samples were then processed as described above. The annual weighted average ^{228}Ra activity of the Mackenzie River was determined to be 16.8 ± 3.7 dpm 100 liter^{-1} (1σ) (fig. S9). Rutgers van der Loeff *et al.* (*19*) measured similar activities in the Lena River (11.1 to 24.9 dpm 100 liter^{-1}) but a significantly higher activity in the Ob River (40.9 ± 3.7 dpm 100 liter^{-1}). The weighted average ^{226}Ra activity of the Mackenzie River was 17.2 ± 4.0 dpm 100 liter^{-1} (1σ), which falls between the activities previously observed in the Ob (27.3 ± 0.6 dpm 100 liter^{-1}) and the Lena (8.5 to 13.1 dpm 100 liter^{-1}) (*19*).

A weighted average of the ^{228}Ra activities from these three rivers was calculated on the basis of the amount of discharge from each river (*26*). This average (24 ± 13 dpm 100 liter^{-1}) was scaled by the runoff estimate of Haine *et al.* (*25*), (4.2 ± 0.42) × 10^{12} m^{3} year^{-1}, to yield a dissolved ^{228}Ra flux of 4.4 × 10^{21} atoms year^{-1}. The error on this flux was calculated by propagating the SDs on each of the individual river activities with the error in the discharge estimate, resulting in a range of possible flux values between 1.8 × 10^{21} and 7.4 × 10^{21} atoms year^{-1}.

In June 2016, samples were collected across the salinity gradient in Kugmallit Bay, part of the East Channel of the Mackenzie River Delta. For salinities up to 15, surface water was collected using a surface submersible pump. For salinities 20 and 25, a Niskin bottle was used to collect water from 5 and 9 m, respectively. Each 20-liter sample was prefiltered through 10-μm and 1-μM Hytrex cartridges to remove suspended sediments before being filtered through an acrylic fiber coated with MnO_2 to scavenge Ra isotopes. Fibers were then rinsed with Ra-free fresh water to remove salt and any remaining sediment, and ashed in a muffle furnace at 820°C for 24 hours. Fiber ash was transferred to polystyrene vials, sealed with epoxy (to prevent ^{222}Rn loss), and counted on high-purity, well-type germanium detectors to measure ^{228}Ra, using the line for ^{228}Ac (911 keV), and ^{226}Ra, using the line for ^{214}Pb (352 keV). Detector efficiencies were determined by measuring ashed fiber standards prepared with a standard solution containing ^{226}Ra and ^{232}Th with daughters in equilibrium.

The amount of ^{228}Ra released from suspended particles was determined to be 0.94 ± 0.25 dpm g^{-1} by dividing the difference between the highest ^{228}Ra activities observed in the estuarine mixing zone (salinity = 3 to 9; 35 ± 4 dpm 100 liter^{-1}, 1σ, n = 3) and the average ^{228}Ra activity in freshwater samples (salinity < 0.5; 19 ± 4, 1σ, n = 7) by the concentration of suspended particles in fresh Mackenzie River water (0.17 ± 0.02 g liter^{-1}). This suspended sediment loading was determined by filtering a known amount of river water through a 0.22-μm polyethersulfone membrane filter and dividing the weight of the dried sediments captured on the filter by the amount of water filtered. Because of the variability in the ^{228}Ra activity of the freshwater endmember (figs. S9 and S10), this estimate of desorbed ^{228}Ra could be improved by further sampling in the Mackenzie River and in Eurasian rivers.

The activity of ^{228}Ra measured in suspended particles was 2.9 ± 0.3 dpm g^{-1}; thus, approximately 32% of the particulate ^{228}Ra desorbed during estuarine mixing; this is similar to previous estimates of ^{228}Ra desorption from riverine particles (*23*). However, this estimate is higher than the percentage of ^{226}Ra released from suspended sediments, which was determined to be 15% based on a difference in freshwater and estuarine activities of 8.2 ± 0.7 dpm ^{226}Ra 100 liter^{-1} and a particulate activity of 3.2 ± 0.1 dpm ^{226}Ra g^{-1}. Because the desorption of both Ra isotopes is expected to be similar, the larger release of ^{228}Ra in the estuarine mixing zone suggests that there is an additional input of ^{228}Ra from bottom sediments (*23*). Here, we do not separate the addition of ^{228}Ra due to desorption from fresh riverine particles and the ^{228}Ra sourced from diffusion from benthic sediments or submarine groundwater discharge; this may overestimate the riverine source of ^{228}Ra and result in a more conservative estimate of the shelf source.

The activity of ^{228}Ra desorbed from suspended particles was scaled by the amount of sediment delivery from Arctic rivers (*26*), 2.8 × 10^{14} g year^{-1}, yielding a desorption flux of 1.1 × 10^{21} atoms year^{-1}. Holmes *et al.* (*26*) did not provide an error estimate for sediment delivery, but the range in compiled literature values is ±70%. By propagating this variability with the errors on the ^{228}Ra measurements, we conclude that the range in the derived desorption flux is 2.5 × 10^{20} to 2.5 × 10^{21} atoms year^{-1}. Adding the dissolved ^{228}Ra flux and the flux of ^{228}Ra from desorption yields a best estimate of the total riverine flux of ^{228}Ra of 5.5 × 10^{21} atoms year^{-1}, with a possible range of 2.0 × 10^{21} to 9.9 × 10^{21} atoms year^{-1}.

Permafrost

Samples of active layer and permafrost sediments were collected from Inuvik and Tuktoyaktuk in the Northwest Territories, Canada, in June 2016. Sediments were dried and homogenized, and three 3-g aliquots from each sample were placed in polystyrene vials for analysis on high-purity well-type germanium γ detectors. For the Tuktoyaktuk permafrost, only one 5-g aliquot of sediment was analyzed due to a scarcity of sediment. The activity of ^{228}Ra in the sediments was measured using the line for ^{228}Ac (911 keV), and ^{226}Ra was measured using the line for ^{214}Pb (352 keV). Similar to the pattern observed for ^{228}Ra, activities of ^{226}Ra were higher in permafrost compared to active layer sediments: Average activities of 2.2 ± 0.3 dpm g^{-1} (1σ, $n = 4$) and 1.8 ± 0.3 dpm g^{-1} (1σ, $n = 6$) were observed in permafrost and active layer sediments, respectively.

Open-water days

The number of open-water days was determined using daily bootstrap sea ice concentrations from Nimbus-7 SMMR and DMSP SSM/I-SSMIS data provided by the National Snow and Ice Data Center (*55*). An open-water day was defined as any day during which the sea ice concentration was less than 15%.

SUPPLEMENTARY MATERIALS

Supplementary material for this article is available at http://advances.sciencemag.org/cgi/content/full/4/1/eaao1302/DC1

fig. S1. Activities of ^{228}Ra in the upper 500 m of the water column with contours indicating the fraction of meteoric water.

fig. S2. Surface water (<15 m) activities of ^{228}Ra from GN01 (circles) shown with activities of ^{228}Ra measured on historical expeditions in the Arctic.

fig. S3. Profiles of ^{228}Ra on the GN01 cruise (2015) compared to the surface samples collected on the GIPY11 cruise (2007) (*16*).

fig. S4. Radium-228 activities in the Transpolar Drift in 1994, 2007, and 2015.

fig. S5. Radium-228 activities in surface waters (2 m) sampled on the GN01 transect in 2015.

fig. S6. Radium-228 activities in surface waters (7 m) on the GIPY11 transect in 2007, measured by Rutgers van der Loeff *et al.* (*16*).

fig. S7. Model of ^{228}Ra and ^{228}Th activities.

fig. S8. Inventory of ^{228}Ra in the top 500 m at each of the stations where water column samples were collected and the bottom depth was ≥1000 m.

fig. S9. Dissolved ^{228}Ra activities measured in the Mackenzie River.

fig. S10. Dissolved ^{228}Ra activities in the Mackenzie River estuary (East Channel).

fig. S11. Satellite-derived record of open water days.

fig. S12. Dissolved ^{226}Ra activities in surface water (<50 m) above 85°N as a function of the fraction of meteoric water in each sample.

fig. S13. Surface water (<15 m) activities of ^{226}Ra from GN01 (circles) shown along with activities of ^{226}Ra measured on historical expeditions in the Arctic.

table S1. Locations of stations used to determine the surface water ^{228}Ra inventory.

table S2. Activities of ^{228}Ra and ^{226}Ra measured in ice-rafted sediments and melted ice.

References (*57*, *58*)

REFERENCES AND NOTES

1. M. Jakobsson, Hypsometry and volume of the Arctic Ocean and its constituent seas. *Geochem. Geophys. Geosyst.* **3**, 1–18 (2002).
2. D. Luo, Q. Wu, H. Jin, S. S. Marchenko, L. Lü, S. Gao, Recent changes in the active layer thickness across the northern hemisphere. *Environ. Earth Sci.* **75**, 555 (2016).
3. M. A. Rawlins, M. Steele, M. M. Holland, J. C. Adam, J. E. Cherry, J. A. Francis, P. Y. Groisman, L. D. Hinzman, T. G. Huntington, D. L. Kane, J. S. Kimball, R. Kwok, R. B. Lammers, C. M. Lee, D. P. Lettenmaier, K. C. McDonald, E. Podest, J. W. Pundsack, B. Rudels, M. C. Serreze, A. Shiklomanov, Ø. Skagseth, T. J. Troy, C. J. Vörösmarty, M. Wensnahan, E. F. Wood, R. Woodgate, D. Yang, K. Zhang, T. Zhang, Analysis of the Arctic system for freshwater cycle intensification: Observations and expectations. *J. Clim.* **23**, 5715–5737 (2010).
4. M. C. Serreze, M. M. Holland, J. Stroeve, Perspectives on the Arctic's shrinking sea-ice cover. *Science* **315**, 1533–1536 (2007).
5. X. Feng, J. E. Vonk, B. E. van Dongen, Ö. Gustafsson, I. P. Semiletov, O. V. Dudarev, Z. Wang, D. B. Montluçon, L. Wacker, T. I. Eglinton, Differential mobilization of terrestrial carbon pools in Eurasian Arctic river basins. *Proc. Natl. Acad. Sci. U.S.A.* **110**, 14168–14173 (2013).
6. P. A. Wheeler, J. M. Watkins, R. L. Hansing, Nutrients, organic carbon and organic nitrogen in the upper water column of the Arctic Ocean: Implications for the sources of dissolved organic carbon. *Deep Sea Res. Part II Top. Stud. Oceanogr.* **44**, 1571–1592 (1997).
7. M. B. Klunder, D. Bauch, P. Laan, H. J. W. de Baar, S. van Heuven, S. Ober, Dissolved iron in the Arctic shelf seas and surface waters of the central Arctic Ocean: Impact of Arctic river water and ice-melt. *J. Geophys. Res.* **117**, C01027 (2012).
8. W. J. Williams, E. C. Carmack, The 'interior' shelves of the Arctic Ocean: Physical oceanographic setting, climatology and effects of sea-ice retreat on cross-shelf exchange. *Prog. Oceanogr.* **139**, 24–41 (2015).
9. E. Carmack, D. C. Chapman, Wind-driven shelf/basin exchange on an Arctic shelf: The joint roles of ice cover extent and shelf-break bathymetry. *Geophys. Res. Lett.* **30**, 1778 (2003).
10. R. M. Key, R. F. Stallard, W. S. Moore, J. L. Sarmiento, Distribution and Flux of ^{226}Ra and ^{228}Ra in the Amazon river estuary. *J. Geophys. Res.* **90**, 6995–7004 (1985).
11. M. A. Charette, P. J. Lam, M. C. Lohan, E. Y. Kwon, V. Hatje, C. Jeandel, A. M. Shiller, G. A. Cutter, A. Thomas, P. W. Boyd, W. B. Homoky, A. Milne, H. Thomas, P. S. Andersson, D. Porcelli, T. Tanaka, W. Geibert, F. Dehairs, J. Garcia-Orellana, Coastal ocean and shelf-sea biogeochemical cycling of trace elements and isotopes: Lessons learned from GEOTRACES. *Philos. Trans. R. Soc. A* **374**, 20160076 (2016).
12. E. Y. Kwon, G. Kim, F. Primeau, W. S. Moore, H.-M. Cho, T. DeVries, J. L. Sarmiento, M. A. Charette, Y.-K. Cho, Global estimate of submarine groundwater discharge based on an observationally constrained radium isotope model. *Geophys. Res. Lett.* **41**, 8438–8444 (2014).
13. D. Kadko, R. Muench, Evaluation of shelf–basin interaction in the western Arctic by use of short-lived radium isotopes: The importance of mesoscale processes. *Deep Sea Res. Part II Top. Stud. Oceanogr.* **52**, 3227–3244 (2005).
14. S. M. Trimble, M. Baskaran, D. Porcelli, Scavenging of thorium isotopes in the Canada Basin of the Arctic Ocean. *Earth Planet. Sci. Lett.* **222**, 915–932 (2004).
15. J. N. Smith, S. B. Moran, R. W. Macdonald, Shelf–basin interactions in the Arctic Ocean based on ^{210}Pb and Ra isotope tracer distributions. *Deep Sea Res. Part I Oceanogr. Res. Pap.* **50**, 397–416 (2003).
16. M. Rutgers van der Loeff, P. Cai, I. Stimac, D. Bauch, C. Hanfland, T. Roeske, S. B. Moran, Shelf-basin exchange times of Arctic surface waters estimated from ^{228}Th/^{228}Ra disequilibrium. *J. Geophys. Res.* **117**, C03024 (2012).
17. F. A. McLaughlin, E. C. Carmack, R. W. Macdonald, J. K. B. Bishop, Physical and geochemical properties across the Atlantic/Pacific water mass front in the southern Canadian Basin. *J. Geophys. Res.* **101**, 1183–1197 (1996).
18. M. B. Alkire, K. K. Falkner, I. Rigor, M. Steele, J. Morison, The return of Pacific waters to the upper layers of the central Arctic Ocean. *Deep. Sea Res. Part I Oceanogr. Res. Pap.* **54**, 1509–1529 (2007).
19. M. Rutgers van der Loeff, S. Kuhne, M. Wahsner, H. Holtzen, M. Frank, B. Ekwurzel, M. Mensch, V. Rachold, ^{228}Ra and ^{226}Ra in the Kara and Laptev seas. *Cont. Shelf Res.* **23**, 113–124 (2003).
20. M. Rutgers van der Loeff, R. M. Key, J. Scholten, D. Bauch, A. Michel, ^{228}Ra as a tracer for shelf water in the Arctic Ocean. *Deep Sea Res. Part II Top. Stud. Oceanogr.* **42**, 1533–1553 (1995).
21. J. L. Sarmiento, C. G. H. Rooth, W. S. Broecker, Radium 228 as a tracer of basin wide processes in the abyssal ocean. *J. Geophys. Res.* **87**, 9694–9698 (1982).
22. P. Schlosser, R. Bayer, G. Bönisch, L. W. Cooper, B. Ekwurzel, W. J. Jenkins, S. Khatiwala, S. Pfirman, W. M. Smethie, Pathways and mean residence times of dissolved pollutants in the ocean derived from transient tracers and stable isotopes. *Sci. Total Environ.* **237–238**, 15–30 (1999).
23. W. S. Moore, H. Astwood, C. Lindstrom, Radium isotopes in coastal waters on the Amazon shelf. *Geochim. Cosmochim. Acta* **59**, 4285–4298 (1995).
24. W. B. Tucker III, A. J. Gow, D. A. Meese, H. W. Bosworth, E. Reimnitz, Physical characteristics of summer sea ice across the Arctic Ocean. *J. Geophys. Res.* **104**, 1489–1504 (1999).
25. T. W. N. Haine, B. Curry, R. Gerdes, E. Hansen, M. Karcher, C. Lee, B. Rudels, G. Spreen, L. de Steur, K. D. Stewart, R. Woodgate, Arctic freshwater export: Status, mechanisms, and prospects. *Glob. Planet Change* **125**, 13–35 (2015).
26. R. M. Holmes, M. T. Coe, G. J. Fiske, T. Gurtovaya, J. W. McClelland, A. I. Shiklomanov, R. G. M. Spencer, S. E. Tank, A. V. Zhulidov, Climate change impacts on the hydrology and biogeochemistry of Arctic rivers, in *Climatic Change and Global Warming of Inland Waters: Impacts and Mitigation for Ecosystems and Societies*, Charles R. Goldman, Richard D. Robarts, Michio Kumagai, Eds. (John Wiley and Sons, 2013), pp. 3–26.
27. R. A. Woodgate, T. J. Weingartner, R. Lindsay, Observed increases in Bering Strait oceanic fluxes from the Pacific to the Arctic from 2001 to 2011 and their impacts on the Arctic Ocean water column. *Geophys. Res. Lett.* **39**, L24603 (2012).
28. R. M. Key, W. S. Moore, J. L. Sarmiento, Transient tracers in the ocean north Atlantic study final data report for ^{228}Ra and ^{226}Ra. Technical Report #92-2 (Ocean Tracer Laboratory, Princeton University, 1992).
29. B. Rudels, M. Korhonen, U. Schauer, S. Pisarev, B. Rabe, A. Wisotzki, Circulation and transformation of Atlantic water in the Eurasian Basin and the contribution of the Fram Strait inflow branch to the Arctic Ocean heat budget. *Prog. Oceanogr.* **132**, 128–152 (2015).
30. H. Lantuit, P. P. Overduin, N. Couture, S. Wetterich, F. Aré, D. Atkinson, J. Brown, G. Cherkashov, D. Drozdov, D. L. Forbes, A. Graves-Gaylord, M. Grigoriev, H.-W. Hubberten, J. Jordan, T. Jorgenson, R. S. Ødegård, S. Ogorodov, W. H. Pollard, V. Rachold, S. Sedenko,

S. Solomon, F. Steenhuisen, I. Streletskaya, A. Vasiliev, The Arctic coastal dynamics database: A new classification scheme and statistics on Arctic permafrost coastlines. *Estuaries Coasts* **35**, 383–400 (2012).
31. F. Günther, P. P. Overduin, A. V. Sandakov, G. Grosse, M. N. Grigoriev, Short- and long-term thermo-erosion of ice-rich permafrost coasts in the Laptev Sea region. *Biogeosciences* **10**, 4297–4318 (2013).
32. R. Stein, R. W. MacDonald, *The Organic Carbon Cycle in the Arctic Ocean* (Springer, 2004).
33. T. C. Lantz, S. V. Kokelj, Increasing rates of retrogressive thaw slump activity in the Mackenzie Delta region, N.W.T., Canada. *Geophys. Res. Lett.* **35**, L06502 (2008).
34. M. T. Jorgenson, Y. L. Shur, E. R. Pullman, Abrupt increase in permafrost degradation in Arctic Alaska. *Geophys. Res. Lett.* **33**, L02503 (2006).
35. S. V. Kokelj, D. Lacelle, T. C. Lantz, J. Tunnicliffe, L. Malone, I. D. Clark, K. S. Chin, Thawing of massive ground ice in mega slumps drives increases in stream sediment and solute flux across a range of watershed scales. *J. Geophys. Res. Earth Surf.* **118**, 681–692 (2013).
36. A. N. Charkin, M. Rutgers van der Loeff, N. E. Shakhova, Ö. Gustafsson, O. V. Dudarev, M. S. Cherepnev, A. N. Salyuk, A. V. Koshurnikov, E. A. Spivak, A. Y. Gunar, I. P. Semiletov, Discovery and characterization of submarine groundwater discharge in the Siberian Arctic seas: A case study in Buor-Khaya Gulf, Laptev Sea. *Cryosphere.* **11**, 2305–2327 (2017).
37. M. A. Walvoord, C. I. Voss, T. P. Wellman, Influence of permafrost distribution on groundwater flow in the context of climate-driven permafrost thaw: Example from Yukon Flats Basin, Alaska, United States. *Water Resour. Res.* **48**, W07524 (2012).
38. L. Rainville, R. A. Woodgate, Observations of internal wave generation in the seasonally ice-free Arctic. *Geophys. Res. Lett.* **36**, L23604 (2009).
39. L. A. Codispoti, V. Kelly, A. Thessen, P. Matrai, S. Suttles, V. Hill, M. Steele, B. Light, Synthesis of primary production in the Arctic Ocean: III. Nitrate and phosphate based estimates of net community production. *Prog. Oceanogr.* **110**, 126–150 (2013).
40. K. R. Arrigo, G. van Dijken, S. Pabi, Impact of a shrinking Arctic ice cover on marine primary production. *Geophys. Res. Lett.* **35**, L19603 (2008).
41. B. A. Bluhm, R. Gradinger, Regional variability in food availability for Arctic marine mammals. *Ecol. Appl.* **18**, S77–S96 (2008).
42. G. A. McFarlane, R. J. Beamish, Climatic influence linking copepod production with strong year-classes in sablefish, *Anoplopoma fimbria*. *Can. J. Fish. Aquat. Sci.* **49**, 743–753 (1992).
43. P. B. Henderson, P. J. Morris, W. S. Moore, M. A. Charette, Methodological advances for measuring low-level radium isotopes in seawater. *J. Radioanal. Nucl. Chem.* **296**, 357–362 (2013).
44. R. M. Key, R. L. Brewer, J. H. Stockwell, N. L. Guinasso Jr., D. R. Schink, Some improved techniques for measuring radon and radium in marine sediments and in seawater. *Mar. Chem.* **7**, 251–264 (1979).
45. M. A. Charette, H. Dulaiova, M. E. Gonneea, P. B. Henderson, W. S. Moore, J. C. Scholten, M. K. Pham, GEOTRACES radium isotopes interlaboratory comparison experiment. *Limnol. Oceanogr. Methods* **10**, 451–463 (2012).
46. I. G. Rigor, J. M. Wallace, R. L. Colony, Response of sea ice to the Arctic oscillation. *J. Clim. Appl. Meteorol.* **15**, 2648–2663 (2002).
47. S. L. Pfirman, R. Colony, D. Nürnberg, H. Eicken, I. Rigor, Reconstructing the origin and trajectory of drifting Arctic sea ice. *J. Geophys. Res.* **102**, 12575–12586 (1997).
48. S. T. Cole, M.-L. Timmermans, J. M. Toole, R. A. Krishfield, F. T. Thwaites, Ekman veering, internal waves, and turbulence observed under Arctic sea ice. *J. Phys. Oceanogr.* **44**, 1306–1328 (2014).
49. A. Kaufman, Y.-H. Li, K. K. Turekian, The removal rates of ^{234}Th and ^{228}Th from waters of the New York Bight. *Earth Planet. Sci. Lett.* **54**, 385–392 (1981).
50. K. Lepore, S. B. Moran, Seasonal changes in thorium scavenging and particle aggregation in the western Arctic ocean. *Deep Sea Res. Part I Oceanogr. Res. Pap.* **54**, 919–938 (2007).
51. R. Newton, P. Schlosser, R. Mortlock, J. Swift, R. MacDonald, Canadian Basin freshwater sources and changes: Results from the 2005 Arctic ocean section. *J. Geophys. Res.* **118**, 2133–2154 (2013).
52. D. Bauch, M. Rutgers van der Loeff, N. Andersen, S. Torres-Valdes, K. Bakker, E. P. Abrahamsen, Origin of freshwater and polynya water in the Arctic ocean halocline in summer 2007. *Prog. Oceanogr.* **91**, 482–495 (2011).
53. M. Baskaran, Interaction of sea ice sediments and surface sea water in the Arctic ocean: Evidence from excess ^{210}Pb. *Geophys. Res. Lett.* **32**, L12601 (2005).
54. H. Eicken, E. Reimnitz, V. Alexandrov, T. Martin, H. Kassens, T. Viehoff, Sea-ice processes in the Laptev Sea and their importance for sediment export. *Cont. Shelf Res.* **17**, 205–233 (1997).
55. J. Cosimo, Bootstrap Sea Ice Concentrations from Nimbus-7 SMMR and DMSP SSM/I-SSMIS, Version 2. Daily. Boulder, Colorado, USA: NASA DAAC at the National Snow and Ice Data Center (2000, updated 2015).
56. B. W. Eakins, G. F. Sharman, Volumes of the World's Oceans from ETOPO1 (NOAA National Geophysical Data Center, Boulder, CO, 2010); available at www.ngdc.noaa.gov/mgg/global/etopo1_ocean_volumes.html.
57. M. P. Bacon, C.-A. Huh, R. M. Moore, Vertical profiles of some natural radionuclides over the Alpha Ridge, Arctic Ocean. *Earth Planet. Sci. Lett.* **95**, 15–22 (1989).
58. R. M. Moore, J. N. Smith, Disequilibria between ^{226}Ra, ^{210}Pb and ^{210}Po in the Arctic Ocean and the implications for chemical modification of the Pacific water inflow. *Earth Planet. Sci. Lett.* **77**, 285–292 (1986).

Acknowledgments: We thank the captain and crew of the U.S. Coast Guard cutter Healy (HLY1502) and the chief scientists, D. Kadko and B. Landing, for support during this expedition. We thank P. Lam, S. Pike, E. Black, M. Heller, Y. Xiang, P. Aguilar, and M. Stephens for their assistance in sample collection on the GN01 expedition; P. Schlosser, R. Newton, T. Koffman, and A. Pasqualini for sharing the water mass fraction data; E. Black and K. Buesseler for sharing the ^{234}Th and ^{238}U data; and L. Kutny for help with the Mackenzie River sampling. **Funding:** This work was funded by NSF awards OCE-1458305 to M.A.C. and OCE-1458424 to W.S.M. The Mackenzie River sampling was supported by a Graduate Student Research Award from the North Pacific Research Board to L.E.K. L.E.K. also acknowledges support from a National Defense Science and Engineering Graduate Fellowship. I.G.R. acknowledges funding by the contributors to the U.S. Interagency Arctic Buoy Program, which include the U.S. Coast Guard, the Department of Energy, NASA, the U.S. Navy, the National Oceanic and Atmospheric Administration, and NSF. **Author contributions:** M.A.C. and W.S.M. designed the GN01 study. L.E.K. carried out GN01 sampling, analyzed samples, and wrote the first draft of the manuscript. W.S.M. and P.B.H. analyzed GN01 samples. I.G.R. determined ice back-trajectories and the number of ice-free days. L.E.K. and M.A.C. designed the Mackenzie River study, and L.E.K. and P.B.H. collected and analyzed samples from that expedition. All authors contributed to the interpretation of the data and the writing of the manuscript. **Competing interests:** The authors declare that they have no competing interests. **Data and materials availability:** Data are available for download from the Biological and Chemical Oceanography Data Management Office (www.bco-dmo.org/dataset/718440). All data needed to evaluate the conclusions in the paper are present in the paper and/or the Supplementary Materials. Additional data related to this paper may be requested from the authors.

Submitted 16 June 2017
Accepted 1 December 2017
Published 3 January 2018
10.1126/sciadv.aao1302

Citation: L. E. Kipp, M. A. Charette, W. S. Moore, P. B. Henderson, I. G. Rigor, Increased fluxes of shelf-derived materials to the central Arctic Ocean. *Sci. Adv.* **4**, eaao1302 (2018).

Increased fluxes of shelf-derived materials to the central Arctic Ocean

Lauren E. Kipp, Matthew A. Charette, Willard S. Moore, Paul B. Henderson and Ignatius G. Rigor

Sci Adv **4** (1), eaao1302.
DOI: 10.1126/sciadv.aao1302